

High-Resolution X-ray Spectroscopy of SS 433 with XRISM

Toshihiro Takagi,^{a,*} Megumi Shidatsu,^a Shogo Kobayashi,^b Yusuke Sakai,^c Yuta Okada,^d Shinya Yamada,^c Yoshihiro Ueda,^d Hideki Uchiyama^e and Marina Yoshimoto^a

^aDepartment of Physics, Ehime University,
2-5 Bunkyo-cho, Matsuyama, Ehime 790-8577, Japan

^bFaculty of Physics, Tokyo University of Science,
1-3 Kagurazaka, Shinjuku-ku, Tokyo 162-8601, Japan

^cDepartment of Physics, Rikkyo University,
3-34-1 Nishi Ikebukuro, Toshima-ku, Tokyo 171-8501, Japan

^dDepartment of Astronomy, Kyoto University,
Kitashirakawa Oiwakecho, Sakyo-ku, Kyoto 606-8502, Japan

^eFaculty of Education, Shizuoka University,
836 Ohya, Suruga-ku, Shizuoka, Shizuoka 422-8529, Japan

E-mail: takagi.toshihiro.bb@ehime-u.ac.jp

SS 433 is a unique Galactic microquasar that exhibits persistent supercritical accretion and relativistic baryonic jets. Its X-ray spectrum shows Doppler-shifted emission lines from bipolar jets, as well as a neutral Fe $K\alpha$ line likely originating from the accretion disk. We observed SS 433 with XRISM in April 2024 over a five-day period, covering both eclipse and non-eclipse phases of the compact object by the companion star. Using Resolve, the X-ray microcalorimeter that delivers unprecedented energy resolution (~ 5 eV at 6 keV) with high sensitivity, we obtained a high-quality X-ray spectrum of SS 433. The Resolve spectrum clearly resolved Doppler-shifted, ionized Fe and Ni K emission lines, along with lower-energy features such as Si and S K lines. Time-resolved spectroscopy revealed that the Fe and Ni K line widths were ~ 20 eV (corresponding to a 1σ velocity dispersion of ~ 1000 km s⁻¹) during eclipse, increasing gradually during egress, and reaching ~ 35 eV (~ 1800 km s⁻¹) outside the eclipse. Furthermore, the time-averaged spectrum outside eclipse showed that Fe and Ni K lines are significantly broader than the Si and S lines, consistent with previous Chandra/HETGS results [1]. This suggests that the velocity dispersion of the jets decreases with distance from the compact object, likely due to progressive collimation or reduced turbulence in the outer regions. We also analyzed the neutral Fe $K\alpha$ line at ~ 6.4 keV. Modeling it with a disk emission line model, we found that it is likely originating from the outermost part of the disk. In this article, we report these results and discuss the spatial structure of the accretion disk and jets inferred from the observed emission lines.

87th Fujihara Seminar The 50th Anniversary Workshop of the Disk Instability Model in Compact Binary Stars (DIM50TH2025)
22-26 September 2025
Tomakomai, Japan

*Speaker

1. Introduction

SS 433 is a remarkable Galactic X-ray binary system that continuously produces bipolar, extended baryonic jets and is uniquely known in our Galaxy for sustaining super-Eddington accretion (see, e.g., [2] for reviews). The jets are launched at a velocity of approximately $0.26 c$ and undergo precession with a period of about 162 days (e.g., [3]; [4]). The system consists of a compact object and an A-type giant companion star in a 13.082-day orbit [5]. Owing to its high orbital inclination (78.8° ; [4]), SS 433 experiences regular eclipses of the compact object and surrounding structures by the companion star. During these eclipse intervals, the innermost X-ray-emitting regions of the jets are obscured, leading to a softer observed X-ray spectrum (e.g., [6]; [7]). Because of its relative proximity, SS 433 serves as an exceptional laboratory for investigating jet structures formed under extremely high mass-accretion conditions.

The X-ray spectrum of SS 433 is characterized by highly ionized emission lines that are blueshifted and redshifted, originating from the approaching and receding jets, respectively. The observed emission is dominated by optically thin thermal plasma radiation from the jets, rather than by direct emission from the accretion disk or its Comptonized component. As the jet plasma propagates outward, it is expected to cool, producing emission at progressively lower energies. Consequently, jet-related X-ray emission provides a powerful diagnostic of the regions closest to the jet base. Using Chandra HETG observations, Namiki et al. (2003) reported that higher-energy emission lines (Fe and Ni) are broader than lower-energy lines (Si and S), suggesting a reduction in radial velocity dispersion along the jet axis. They interpreted this trend as evidence for gradual jet collimation (i.e., a decreasing jet opening angle) at distances of order $\sim 10^{12}$ cm from the compact object. The robustness of this conclusion, however, has been debated. Because of limited spectral resolution and photon statistics, the result relied on empirical Gaussian fits to multiple lines of different ionization stages, assuming identical line widths. As noted by Marshall et al. (2013), the FeXXV He α line at 6.7 keV, which is the strongest line above 5 keV and a key contributor to the inferred velocity dispersion, may be affected by unresolved line blending, potentially leading to an overestimate of the intrinsic width. Accurate measurements of individual line widths therefore require sufficient spectral resolution to resolve these components. Establishing the true structure of the jets thus demands observations with both higher energy resolution and improved statistics.

Beyond the jet-origin emission lines, nearly stationary and narrow neutral iron emission has also been reported (e.g., [8]; [9]), indicating the presence of cold material surrounding the X-ray-emitting regions. The neutral iron line (FeI K α) has been proposed to arise either from the accretion disk around the compact object or from winds launched from the disk [8]. Broadband X-ray observations with NuSTAR further suggest that, in addition to the jet component, a reflection component contributes to the continuum emission and can naturally account for the neutral iron lines [10]. An alternative scenario, in which neutral lines are produced through scattering of emission from the hottest jet regions by the disk wind, was proposed by Medvedev et al. (2018). Given that the FeI K α line is intrinsically very narrow, resolving it also requires high energy resolution.

In this study, we address these issues using the X-Ray Imaging and Spectroscopy Mission (XRISM; [11]), equipped with the X-ray microcalorimeter Resolve [12]. Resolve provides unprecedented energy resolution along with substantial effective area, particularly in the Fe K band. This capability allows us to separate the Fe K emission lines from the jets and the FeI K α line in SS 433,

enabling precise measurements of their intrinsic widths. In addition, we can investigate temporal variations in the ionized Fe K lines from jets during eclipse and non-eclipse phases. If the line-of-sight velocity dispersion of the jets decreases with increasing distance from the compact object, broader lines are expected outside eclipse, when the inner jet regions are visible, than during eclipse, when they are obscured. This offers a new constraint on the jet structure, complementary to comparisons of jet emission lines across different energy bands as performed by Namiki et al. (2003). In this article, we summarize the key results from our Resolve spectroscopy of SS 433. For more details of the analyses and discussions, we refer the readers to Shidatsu et al. (2025) and Takagi et al. (2025, in press). Unless stated otherwise, all quoted uncertainties correspond to 90% confidence intervals for a single parameter.

2. Observation and Data Reduction

The XRISM observation was conducted between 2024 April 10 at 13:41 UT and April 15 at 10:32 UT (OBSID=300041010), yielding a total effective exposure of approximately 200 ks. During this observation, the X-ray microcalorimeter Resolve was operated with the gate valve closed condition and without any additional optical blocking filters. Based on the ephemeris of Goranskij (2011), the observation covers the orbital phase range $\phi_{\text{orb}} = 0.003\text{--}0.375$, where $\phi_{\text{orb}} = 0$ corresponds to the inferior conjunction of the companion star, and thus includes the eclipse interval. The jet precession phase during the observation is predicted, using the ephemeris of Gies et al. (2002), to be $\phi_{\text{jet}} = 0.214\text{--}0.244$, where $\phi_{\text{jet}} = 0$ denotes the epoch at which the approaching jet is most closely aligned with the line of sight, but the actual phase was slightly shifted from this predicted range [16]. The data reduction was performed in accordance with the XRISM Quick Start Guide v2.3¹. Spectral analysis was restricted to energies above 2 keV, since lower-energy X-rays are largely attenuated by the closed gate valve. We did not subtract contributions from the non-X-ray background (NXB), cosmic X-ray background (CXB), or Galactic ridge X-ray emission (GRXE), as these components were confirmed to be negligible for this dataset.

3. Analysis and Results

Figure 1 shows the Resolve light curve in 2–10 keV over the entire observation period. During our observation, the source intensity remained at a low level at the beginning and then gradually increased, reaching a higher level at approximately $\sim 1.3 \times 10^5$ s after the start of the observation, corresponding to an orbital phase of $\phi_{\text{orb}} \sim 0.13$. Taking this temporal behavior into account, we define the initial $\sim 1.3 \times 10^5$ s interval as the eclipse phase, and the subsequent interval as the non-eclipse phase.

3.1 Time Variation of the Velocity Dispersion in the Fe K Band

To minimize the apparent line broadening caused by jet precession, we divided the Resolve dataset into individual continuous exposures and performed spectral fitting using the time-averaged spectrum of each segment. In total, 95 segments were obtained, each with a typical net exposure

¹<https://heasarc.gsfc.nasa.gov/docs/xrism/analysis/quickstart/>

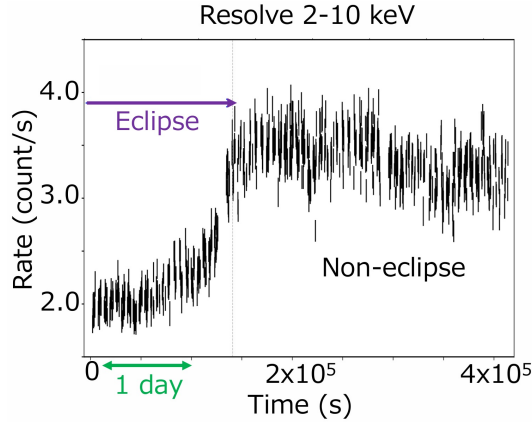


Figure 1: Resolve light curves with 512 s bins. The errors indicate 1σ statistical uncertainties.

of approximately 3500 s. Figure 2 presents representative spectra from the eclipse and non-eclipse phases. Both spectra exhibit Doppler-shifted emission lines of highly ionized Fe and Ni originating from the approaching and receding jets, as well as a narrow FeI $K\alpha$ line. To model the jet emission, we employed the `bvapec` model, which is an optically thin, collisionally ionized plasma model based on APEC [17], allowing for variable elemental abundances and additional Gaussian velocity broadening. Two `bvapec` components were combined to represent the approaching and receding jets (hereafter referred to as `bvapec_b` and `bvapec_r`, respectively). We linked all the parameters except for the Doppler shift between the `bvapec_b` and `bvapec_r` components. We adopted the elemental abundance tables by Lodders et al. (2009) and the photoelectric cross sections by Verner et al. (1996). In addition, a narrow Gaussian component was included to model the FeI $K\alpha$ line, with its centroid energy and 1σ width fixed at 6.4 keV and 10 eV, respectively. The full spectral model is therefore expressed as `bvapec_r + bvapec_b + gauss`.

In Figure 2, we show the best-fit models for the representative eclipse and non-eclipse spectra. We find that the jet emission lines are significantly broader during the non-eclipse phase compared to the eclipse phase. The inferred velocity dispersion of the jet (σ_{jet}) is approximately 1000 km s^{-1} in the eclipse phase and increases to about 1700 km s^{-1} in the non-eclipse phase. Figure 3 illustrates the temporal evolution of the velocity dispersion throughout the observation. The velocity dispersion shows a gradual increase during the egress phase ($\sim 5 \times 10^4 \text{ s}$ to $\sim 1.2 \times 10^5 \text{ s}$), coinciding with the gradual rise in flux (figure 1), and remains approximately constant during the non-eclipse phase.

3.2 Comparison of the Velocity Dispersions in the Fe K and Si/S K Bands

We further investigated the behavior of the velocity dispersion using an alternative method by comparing emission lines in the Fe K band (5.5–9 keV) with those in the Si/S K band (2–4 keV), following the approach adopted by Namiki et al. (2003). As discussed in the previous section, integrating over longer time intervals can enhance line broadening caused by Doppler shifts associated with jet precession and nodding motion; however, as shown below, we nevertheless obtain results that support a decrease in the line-of-sight velocity dispersion toward larger distances from the compact object.

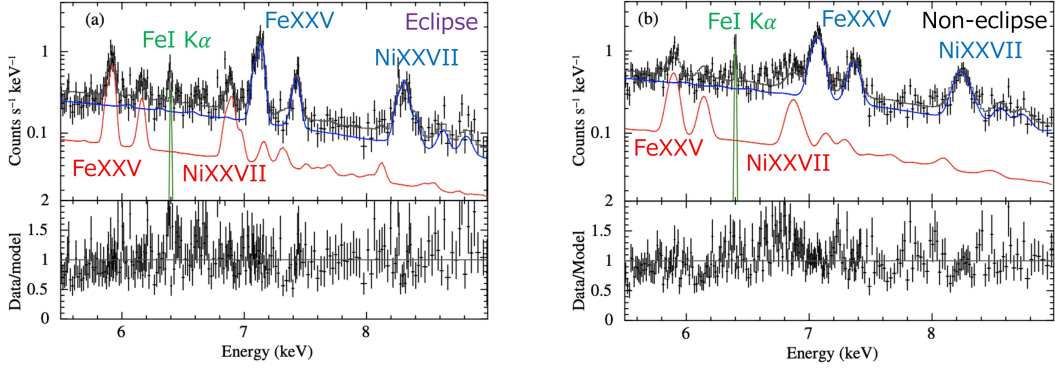


Figure 2: Panels (a) and (b) display representative spectra obtained during the eclipse and non-eclipse phases, respectively, together with their best-fit models. The blue, red, and green curves indicate the contributions from the approaching jet, the receding jet, and the narrow FeI $K\alpha$ line, respectively. The ratios of the data to the model are shown in the lower panels.

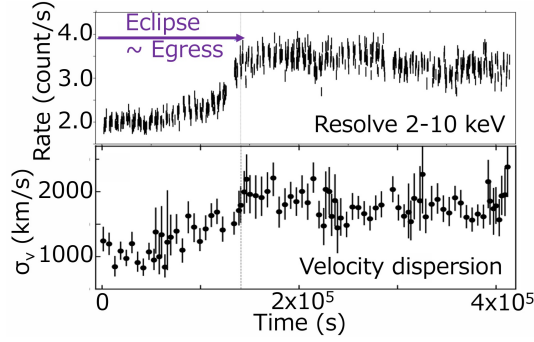


Figure 3: (Top) Same as figure 1. (Bottom) Evolution of the jet velocity dispersion.

To ensure adequate photon statistics while avoiding jet obscuration during the eclipse and reducing line broadening due to precession, we selected data in the orbital phase range $\phi_{\text{orb}} = 0.13\text{--}0.20$, corresponding to a net exposure of approximately 40 ks. During this interval, the temporal variation in the Doppler shifts of the approaching and receding jets was relatively small ($\Delta z_b \sim -0.006$ and $\Delta z_r \sim 0.008$), as estimated from the time-resolved spectral analysis. We applied the same spectral model used in the time-resolved analysis, but additionally included the neutral absorption model `tbabs` to account for interstellar absorption, which primarily affects the spectrum at lower energies. The elemental abundance tables and photoelectric cross sections adopted for `tbabs` were identical to those used for `bvapec`. The model was fitted independently to the spectra in the 2–4 keV and 5.5–9 keV bands. We found that allowing the velocity dispersions of the `bvapec_r` and `bvapec_b` components to vary independently led to a significant improvement in the fit quality in the 5.5–9 keV band, whereas no such improvement was seen in the 2–4 keV band. Accordingly, we allowed the velocity dispersions to be unlinked only for the former energy range.

Figure 4(a) presents the observed spectrum and best-fit model in the 5.5–9 keV range. While the model broadly reproduces the overall spectral shape in this band, notable residuals remain around 6.2–7.0 keV, similar to those observed in the time-averaged spectra. To improve the fit, we

introduced two additional Gaussian components centered at approximately 6.4 keV and 6.9 keV. The spectrum and best-fit model in the 2–4 keV band are shown in figure 4(b). The derived velocity dispersion in the 2–4 keV band ($\sigma_{\text{jet}} = 1300^{+300}_{-400}$ km s⁻¹) was found to be significantly smaller than that of the approaching jet measured in the 5.5–9 keV band (1900 ± 80 km s⁻¹), but comparable to that of the receding jet in the same energy range (1400 ± 200 km s⁻¹).

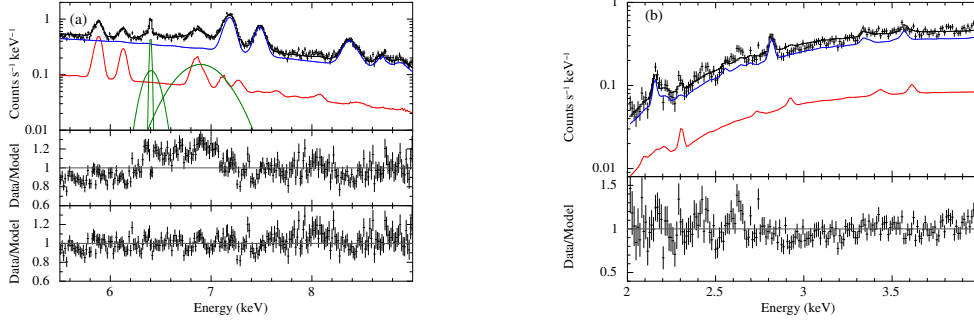


Figure 4: The time-averaged spectra obtained during $\phi_{\text{orb}} = 0.13\text{--}0.20$ in (a) the 5.5–9 keV band and (b) the 2–4 keV band, together with their best-fit models. The contributions from the approaching jet, receding jet, and Gaussian line components are indicated by blue, red, and green curves, respectively. The middle and bottom panels in panel (a) display the data-to-model ratios for the best-fit models without and with the inclusion of the two broad Gaussian components, respectively. The bottom panel in panel (b) also shows the data-to-model ratios for the best-fit model.

3.3 Modeling the FeI $K\alpha$ Line Profile

To examine the FeI $K\alpha$ emission line in detail, we carried out spectral modeling. We restricted the analysis to the 6.3–6.5 keV energy range in order to isolate the FeI $K\alpha$ feature and minimize contamination from jet-related emission lines. Owing to the high energy resolution of Resolve (~ 5 eV), representing the FeI $K\alpha$ line with a single Gaussian component may be insufficient, making it necessary to account for its intrinsic fine structure. Accordingly, we adopted a phenomenological model consisting of a combination of seven Lorentzian components derived from laboratory measurements ([21]; hereafter referred to as the Hölzer_Fe model). The line parameters, including natural broadening, were taken from Hölzer et al. (1997). The relative intensities of the α_{12} , α_{13} , α_{14} , α_{21} , α_{22} , and α_{23} components were fixed at 0.655, 0.381, 0.338, 0.745, 0.237, and 0.234, respectively, relative to the α_{11} component [21], while the normalization of α_{11} was left as a free parameter. The underlying continuum was modeled with a power-law, and the Doppler shift of the FeI $K\alpha$ line complex was incorporated using the `zshift` model.

Figure 5 presents the observed spectrum together with the best-fit model, which corresponds to a Hölzer_Fe profile convolved with Keplerian broadening from an accretion disk, expressed as `power-law + zshift * rdblur * Hölzer_Fe`. The `rdblur` component accounts for relativistic line broadening expected from a standard accretion disk [22]. In this modeling, the inner disk radius R_{in} was treated as a free parameter. The disk inclination was fixed at 68° , assuming that the disk is orthogonal to the jet axis and shares its precessional motion. From this analysis, we inferred an inner disk radius on the order of $10^{5-6} R_{\text{g}}$.

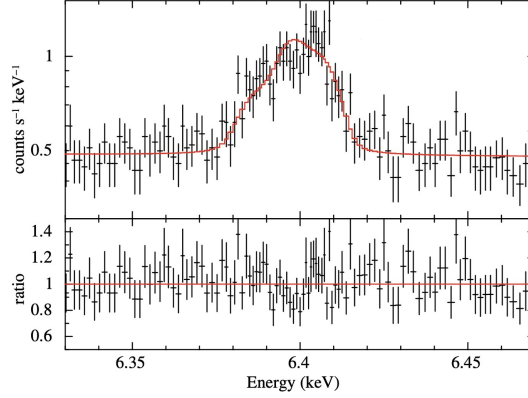


Figure 5: (Top panel) Resolve 6.3–6.5 keV spectrum and the best-fit model. (Bottom panel) residuals between the data and the models. The error bars represent 1σ statistical uncertainty.

4. Discussion and Conclusion

Owing to the high energy resolution and large effective area of XRISM/Resolve, we were able to clearly resolve Doppler-shifted emission lines from the jets, including the FeXXVI Ly α line, which suffers relatively little from line blending. Our time-resolved spectral analysis in the Fe K band shows that the jet emission lines are markedly broader during the non-eclipse phase than during the eclipse phase. This behavior, together with the comparison of the widths of the Fe/Ni and Si/S lines for the approaching jet component in the time-averaged spectrum, indicates that the velocity dispersion decreases as the jet plasma propagates outward. Namiki et al. (2003) attributed this behavior to progressive collimation of the jets, corresponding to a gradual reduction in their opening angle. If valid, our results imply that relativistic jets undergo additional collimation after being launched and accelerated. An alternative explanation is that the jet plasma exhibits stronger turbulence in hotter regions than in cooler ones. Indeed, recent hydrodynamical simulations of supercritical accretion flows predict the presence of turbulent structures in the vicinity of the jets (e.g., [23]). In addition, we find that the Fe/Ni line width of the approaching jet is broader than that of the receding jet. This can be explained if the receding jet was more strongly obscured by the accretion disk, given that the approaching jet was tilted toward the observer during this observation.

Using XRISM/Resolve, we have also successfully resolved the FeI K α line. Its measured width of approximately 7 eV is significantly larger than the intrinsic line width determined from laboratory measurements [21]. If this emission arises from a standard accretion disk, the inferred width corresponds to an emitting radius of order $10^{5-6} R_g$. This result suggests that the FeI K α line is produced in the outer regions of the accretion disk or in a disk wind enveloping the disk.

All these results presented above were made possible by the unprecedented line-resolving power of Resolve. Observations of SS 433 at other orbital and precessional phases are expected to further advance our understanding of the structure and dynamics of the jets and the supercritical accretion flow.

References

- [1] Namiki, M., Kawai, N., Kotani, T., & Makishima, K. 2003, PASJ, 55, 281
- [2] Fabrika, S. 2004, *Astrophys. Space Phys. Res.*, 12, 1
- [3] Abell, G. O., & Margon, B. 1979, *Nature*, 279, 701
- [4] Margon, B., & Anderson, S. F. 1989, *ApJ*, 347, 448
- [5] Goranskij, V. 2011, *Peremennye Zvezdy*, 31, 5
- [6] Kawai, N., Matsuoka, M., Pan, H.-C., & Stewart, G. C. 1989, PASJ, 41, 491
- [7] Marshall, H. L., Canizares, C. R., Hillwig, T., et al. 2013, *ApJ*, 775, 75
- [8] Kotani, T., Kawai, N., Matsuoka, M., & Brinkmann, W. 1996, PASJ, 48, 619
- [9] Medvedev, P. S., Khabibullin, I. I., Sazonov, S. Y., Churazov, E. M., & Tsygankov, S. S. 2018, *Astronomy Letters*, 44, 390
- [10] Middleton, M. J., Walton, D. J., Alston, W., et al. 2021, *MNRAS*, 506, 1045
- [11] Tashiro, M., Maejima, H., Toda, K., et al. 2020, in *Society of Photo-Optical Instrumentation Engineers (SPIE) Conference Series*, Vol. 11444, *Space Telescopes and Instrumentation 2020: Ultraviolet to Gamma Ray*, ed. J. W. A. den Herder, S. Nikzad, & K. Nakazawa, 1144422
- [12] Ishisaki, Y., Kelley, R. L., Awaki, H., et al. 2022, in *Society of Photo-Optical Instrumentation Engineers (SPIE) Conference Series*, Vol. 12181, *Space Telescopes and Instrumentation 2022: Ultraviolet to Gamma Ray*, ed. J. W. A. den Herder, S. Nikzad, & K. Nakazawa, 121811S
- [13] Shidatsu, M., Kobayashi, S., Sakai, Y., et al. 2025, PASJ, 77, 1313
- [14] Takagi, T., Shidatsu, M., Yuta, O., Sakai, Y., & Yamada, S. 2025, PASJ, in press
- [15] Gies, D. R., McSwain, M. V., Riddle, R. L., et al. 2002, *ApJ*, 566, 1069
- [16] Sakai, Y., Yamada, S., Okada, Y., et al. 2025, PASJ in press
- [17] Smith, R. K., Brickhouse, N. S., Liedahl, D. A., & Raymond, J. C. 2001, *ApJL*, 556, L91
- [18] Lodders, K., Palme, H., & Gail, H. P. 2009, *Landolt Börnstein*, 4B, 712
- [19] Verner, D. A., Ferland, G. J., Korista, K. T., & Yakovlev, D. G. 1996, *ApJ*, 465, 487
- [20] Medvedev, P. S., Khabibullin, I. I., & Sazonov, S. Y. 2019, *Astronomy Letters*, 45, 299
- [21] Hölzer, G., Fritsch, M., Deutsch, M., Härtwig, J., & Förster, E. 1997, *Phys. Rev. A*, 56, 4554
- [22] Fabian, A. C., Rees, M. J., Stella, L., & White, N. E. 1989, *MNRAS*, 238, 729
- [23] Jiang, Y.-F., Stone, J. M., & Davis, S. W. 2014, *ApJ*, 796, 106